

Biomaterials Science

Accepted Manuscript

This article can be cited before page numbers have been issued, to do this please use: X. Wang, L. Qiu, C. Wang, Z. Gao, S. Zhou, P. Cui, P. Jiang, H. Hu, X. Ni, X. Du, J. Wang and J. Xia, *Biomater. Sci.*, 2022, DOI: 10.1039/D1BM01533H.



This is an Accepted Manuscript, which has been through the Royal Society of Chemistry peer review process and has been accepted for publication.

Accepted Manuscripts are published online shortly after acceptance, before technical editing, formatting and proof reading. Using this free service, authors can make their results available to the community, in citable form, before we publish the edited article. We will replace this Accepted Manuscript with the edited and formatted Advance Article as soon as it is available.

You can find more information about Accepted Manuscripts in the [Information for Authors](#).

Please note that technical editing may introduce minor changes to the text and/or graphics, which may alter content. The journal's standard [Terms & Conditions](#) and the [Ethical guidelines](#) still apply. In no event shall the Royal Society of Chemistry be held responsible for any errors or omissions in this Accepted Manuscript or any consequences arising from the use of any information it contains.

Nanodot-doped peptide hydrogel for antibacterial phototherapy and wound healing

View Article Online
DOI: 10.1039/D1BM01533H

Xuan Wang,^{1, #} Lin Qiu,^{1, #} Cheng Wang,¹ Zihan Gao,¹ Shuwen Zhou,¹ Pengfei Cui,¹ Pengju Jiang,¹ Huaanzi Hu,¹ Xinye Ni,^{2, *} Xuancheng Du,³ Jianhao Wang,^{1, *} Jiang Xia^{4, *}

¹ School of Pharmacy, Changzhou University, Changzhou, Jiangsu 213164, China.

² The Affiliated Changzhou No. 2 People's Hospital of Nanjing Medical University, Changzhou, Jiangsu, P. R. China

³ Institute of Advanced Interdisciplinary Science, School of Physics, Shandong University, Jinan 250100, China.

⁴ Department of Chemistry, the Chinese University of Hong Kong, Shatin, Hong Kong SAR, China.

These authors contributed equally to this work.

* To whom correspondence may be addressed. Xinye Ni, nxy@njmu.edu.cn; Jianhao Wang, minuswan@163.com; Jiang Xia, jiangxia@cuhk.edu.hk.

ABSTRACT

Bacterial infection of the wounds delays the healing process, increases the risk of becoming chronic trauma associated with pain and complications, and offers a breeding ground for drug-resistant bacteria. A rapid, effective eradication of the bacterial species in the wound area is thus important. Herein, we designed a phototherapeutic antibacterial platform based on peptides and copper sulfide nanodots (CuS NDs) to render multi-mechanistic eradication of bacteria colonized on the wound surface. The antimicrobial peptide weaves into a network in the form of a hydrogel, which supports CuS NDs to generate heat and produce reactive oxygen species (ROS) under the irradiation of near infrared light (NIR). The heat and ROS generated *in situ* act as non-contact based antibacterial factors, and together with contact-based antimicrobial peptide cause irreversible membrane destruction, cell content

damage, and thermal ablation of the bacteria. Lastly, nanodot-doped peptide hydrogel combined with collagen showed complete bacterial elimination and significantly accelerated wound healing in splint fixed mice infection model.

View Article Online
DOI: 10.1039/C1BM01533H

KEYWORDS

Antimicrobial peptide hydrogel, copper sulfide nanodots, phototherapeutic antibacterial, skin infection

INTRODUCTION

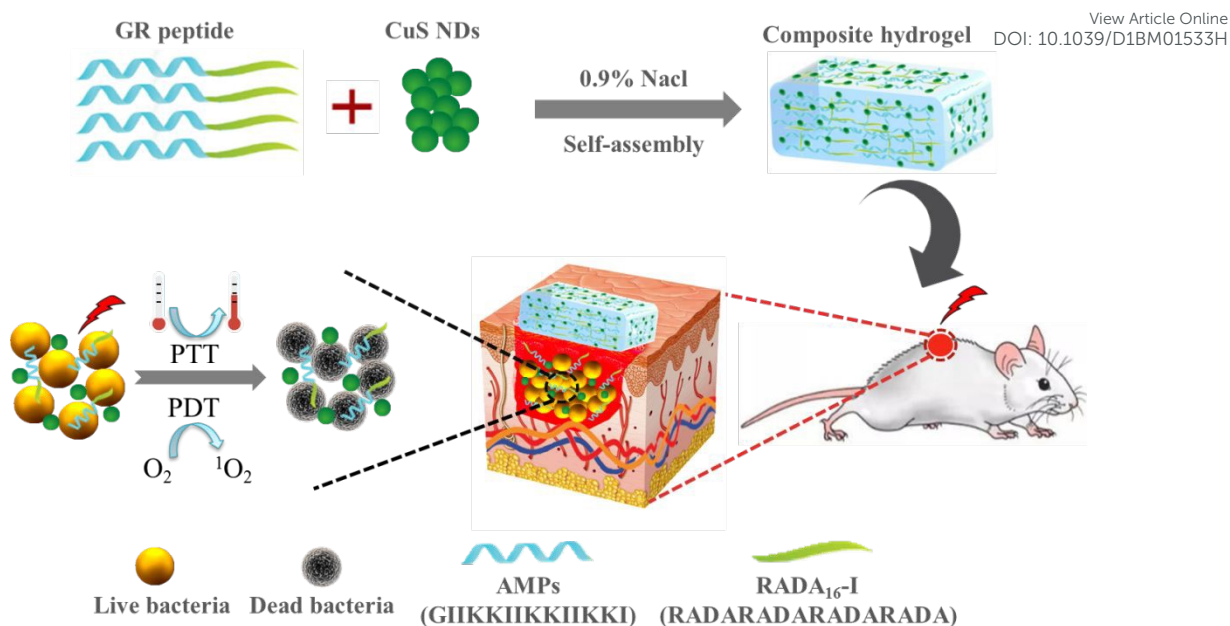
As the barrier between the internal organs and the outside world, skin has important physiological functions such as protection, regulation, metabolism and so on. Because the skin is in direct contact with the outside world, it is vulnerable to different types of damage.¹⁻³ Wounds will develop when damages occur. Skin has an impressive self-healing capability through a four-stage process including hemostasis, inflammation, proliferation and remodeling. This process however can be interfered by external factors, and together with pathological factors, chronic wounds can occur, especially in vulnerable patients.⁴⁻⁷ Bacterial infection is one of the external factors that can deteriorate the wounds, delay the healing process and incur infection-related complications, such as septicemia, acute renal failure and even death.⁸⁻¹² Antibiotics are usually used to fight with bacterial infections, but the rapid emergence of drug-resistant bacteria dwarfs the antibiotic drug development pipeline.^{13,14} It is predicted that although the global expenditure on the treatment of drug-resistant bacteria will climb up to \$100 trillion by 2050, the mortality will still be millions.¹⁵

New antibacterial regimens with mechanisms different from currently existing antibiotics as antibacterial alternatives hold the key towards the battle against drug resistance.¹⁶ In recent years, phototherapeutic antimicrobial strategies based on photo-active materials and photocatalysis have received increasing attention due to their safety, controllability and non-invasiveness.^{17,18} Among them, metal nanomaterials are widely explored as the one of the most promising phototherapeutic agents because their composition and configuration can be easily adjusted to achieve the desired functions. Phototherapeutic agents respond to light

irradiation to produce reactive oxygen species (ROS) that damage cell membranes or generate heat at a focal point, thus killing bacteria or inhibiting bacterial growth through mechanisms that are completely different from that of antibiotics.^{19,20} As a semiconductor phototherapeutic agent, copper sulfide (CuS) not only converts light to thermal energy by d-d energy band transition, but also produces highly toxic ROS, which render them a promising new type of antibacterial biomaterials.^{21,22}

Antimicrobial peptides (AMPs) are also a powerful weapon against multidrug resistance in the "post-antibiotic era".²³⁻²⁶ Their unique mechanism of membrane destruction often makes them broad-spectrum antimicrobials and as the membrane is so essential to bacterial cells, resistance development will be relatively rare. Therefore, we speculate that the combination of low temperature photothermal and photodynamic therapy with antimicrobial peptides may achieve an added effect of " $1+1 > 2$ ", that is, the former reduces the viability of bacterial cells and opens the gap in the biofilm, while the latter carries out physical infiltration for the final effective harvest. Together with the fabrication of AMPs into the form of a three-dimensional (3D) porous hydrogel material, nanoparticle-doped peptide hydrogel will be an ideal dressing material for the infected wounds, which can keep the skin hydrated, promote the wound healing, and eradicate bacterial infection at the wounds.

Taken together, in this study we fuse antimicrobial peptides with a gel-forming RADA₁₆-I peptide to form hydrogel scaffolds, and dope copper sulfide nanodots (CuS NDs) in the hydrogel for antibacterial phototherapy and wound healing. The antimicrobial peptide hydrogel provides a contact-based antibacterial matrix and upon light irradiation, CuS NDs release non-contact-based antibacterial agents. The three antibacterial factors combined rapidly kill bacterial cells, and promote wound healing in a mouse model. The nanodot-doped peptide hydrogel thus represents a multi-mechanistic platform for infection control in wounds (Scheme 1).



Scheme 1. Schematic illustration of CuS NDs-doped peptide hydrogel for antibacterial phototherapy and wound healing.

Experimental Section

Materials

Fmoc-protected amino acids and coupling reagents were purchased from GL Biochem Ltd. H-Rink amide ChemMatrix resin, 3-(4,5-Dimethylthiazol-2-yl)-2,5-diphenyltetrazolium bromide (MTT reagent), crystal violet stain solution, phosphate-buffered saline (PBS buffer), Luria–Bertani broth (LB) medium and dimethyl sulfoxide (DMSO) were purchased from Sigma-Aldrich. Live/dead bacteria viability kit, Dulbecco's modified Eagle's medium (DMEM) were purchased from ThermoFisher. Recombinant human collagen type III (gel) was obtained from Jiangsu Chuangjian Medical Technology Co., Ltd. All other chemicals were obtained from Adamas-beta and used without further purification. Deionized (DI) water (Millipore Milli-Q grade, 18.2 MΩ) was used in all experiments.

Preparation and characterization of peptide-based hydrogels. Peptide (GIIKKIHKIIKKIGRADARADARADARADA-NH₂) was synthesized by Fmoc solid phase synthesis using Rink-Amide-ChemMatrix resin and chemically modified α-amino acids as raw materials. The peptides were cleaved from the resin by trifluoroacetic acid mixed solution (TFA:EDT:TIS:H₂O=94:2.5:1:2.5), precipitated and centrifuged with ice-cold diethyl ether and dissolved in DI water. The product was purified by semi-preparative high

performance liquid chromatography (HPLC, Shimadzu LC-8A, JEOL, Japan) and verified by LC-MS after freeze-drying. To prepare peptides-based hydrogel, the purified peptide powder was dissolved in normal saline (20 mg/mL) and gelled at 37 °C. The gel was verified by small bottle inversion method. The drug-loaded peptides-based hydrogel can be prepared by dissolving the drug and the peptide powder in normal saline. The mechanical properties and shear thinning ability of GR polypeptide hydrogel were evaluated by shock rheology test. The microstructure of GR peptide hydrogel was observed by atomic force microscope (AFM, NANOWIZARD3, JPK, Germany) and transmission electron microscope (TEM, Tecnai G20, FEI, USA). The secondary structure and intermolecular force of GR hydrogel were studied by Fourier transform infrared spectroscopy (FT-IR, Nicolet iS50, Thermo fisher, USA) and fluorescence spectra.

Preparation of composite hydrogels. CuS NDs was dissolved in normal saline in advance, and then saline containing CuS NDs was dissolved in GR peptide powder, which was completely dissolved by ultrasound, and composite hydrogel was formed after standing at 37 °C.

Preparation and characterization of CuS Nanodots. CuS nanodots (CuS NDs) are synthesized according to the previously published method. Briefly, 21 mg $\text{CuCl}_2 \cdot 2\text{H}_2\text{O}$ and 60 mg polyvinylpyrrolidone (PVP, M.W. 40000) were added into 5 mL DI water. After stirring clarified, 30 mg $\text{Na}_2\text{S} \cdot 9\text{H}_2\text{O}$ were added into the mixture. Then the mixed solution was heated to 90 °C for 15 min to obtain dark green solution. CuS NDs can be obtained after 24 hours of dialysis in DI water. The particle size and dispersion of CuS NDs were measured by Malvern particle size analyzer (ZS90, Malvern, UK). The morphology of CuS NDs was observed by TEM. A multi-functional enzyme labeling instrument (Synergy NEO, BioTek, USA) was used to measure the ultraviolet absorption spectrum of CuS NDs.

Related photothermal properties of CuS NDs. To measure the related photothermal properties of CuS NDs, different concentrations of CuS NDs (0, 0.5, 0.75, 1.0, 1.25 mg/mL) were irradiated with NIR laser (808 nm, 1.8 W/cm²) for 6 min, and the temperature was recorded every 1 min. Then CuS NDs (1 mg/mL) was irradiated with different laser power (1.5, 1.8, 2.1, 2.4 W/cm²), and the temperature change was recorded in the same way. The photothermal stability of CuS NDs was evaluated by repeatedly measuring the photothermal

behavior of on/off for 5 times. DPBF was added to CuS NDs solution as an indicator. After 6 min in NIR laser (808 nm, 1.8 W/cm²), the changes of color and UV-Vis spectrum were observed to determine the production of ROS.

Bacterial culture. *S. aureus* (ATCC6538) and *E. coli* (ATCC8739) were selected in the experiment. The bacteria were cultured overnight in LB broth in shaker (37 °C, 250 rpm). After centrifugation, the bacteria entered the exponential growth phase. The concentration of bacteria was determined by measuring its optical density (OD) value at 600 nm. When OD₆₀₀ was 0.1, the concentrations of *S. aureus* and *E. coli* were 2×10^8 and 1.5×10^8 CFU/mL, respectively.

In vitro photodynamic antimicrobial activity. The 250 μL of sample was co-cultured with 1 mL bacteria for 1 h (heat-based sterilization required NIR laser to irradiate 6 min before culture). The concentration of GR peptide was 20 μM, and the concentrations of CuS NDs and *S. aureus* were 1 mg/mL and 2×10^8 CFU/mL (OD₆₀₀ = 0.1), respectively. Then the diluted mixed bacterial solution was inoculated on agar plate and cultured at 37 °C for 16 h. The antibacterial property of the sample was evaluated by colony number. Moreover, the inhibitory effect of GR hydrogel on the growth curve of *S. aureus* was determined on 96-well plate. Briefly, the mixed solution of GR hydrogel and *S. aureus* was incubated at 37 °C on a 96-well plate, and the OD₆₀₀ value of each well was recorded every 1 hour to evaluate the inhibitory effect of GR hydrogel on the growth of *S. aureus*.

Inhibition of the biofilm formation. *S. aureus* in logarithmic growth phase and GR hydrogel were added to the 96-well plate and co-cultured at 37 °C for 48 h. Then discarding the upper culture medium, PBS was added to gently wash off the suspended bacteria, and 1% (v/v) crystal purple ethanol solution was added and reacted for 20 min. Finally, the excess crystal violet solution was washed off with PBS, and the bottom residue was dissolved with 80% ethanol solution to determine its absorbance at 590 nm. The inhibitory effect of biofilm was evaluated according to the absorbance of each group.

Biofilm destruction. *S. aureus* in logarithmic growth phase was added to the 96-well plate and cultured at 37 °C for 48 h to form a complete biofilm. Then GR and composite hydrogels were added, in which the hydrogel loaded with CuS NDs irradiated 6 min with NIR (808 nm,

1.8 W/cm²), the 96-well plate was returned to the incubator for culture. The remaining steps are the same as above. View Article Online
DOI: 10.1039/C1BM01533H

Live/Dead bacterial staining analysis. The bacteria were co-incubated with GR hydrogel, and the upper culture medium was removed after freeze centrifugation. The bottom precipitate used SYTO 9 / PI solution to react 30 min in the dark. 30 μ L mixed liquid were taken on the slide and observed by confocal fluorescence microscope. Living cells are stained green by SYTO 9, while dead cells are stained red by PI.

Hemolysis experiment. Fresh blood was extracted from the eyeballs of healthy mice and red blood cells were separated by freeze centrifugation. The PBS solution of 20% (v/v) red blood cells was mixed with different concentrations of GR peptides. 1% TritonX-100 as the positive hemolysis control and PBS as the negative control. All samples were incubated at 37 °C for 2 hours, and then the supernatant was obtained by freeze centrifugation to measure the absorbance at 540 nm.

Cytotoxicity. The toxicity of GR peptide on mouse fibroblasts (*L929s*) was detected by MTT. *L929s* cells were inoculated in 96-well (10⁴/well) plates and cultured overnight. Then different concentrations of GR peptides were co-incubated with cells. After 24 hours, MTT solution was added, and the cell survival rate was measured by measuring the absorbance of each well at 490 nm.

Mouse wound model of *S. aureus* infection. Female mice (Balb/c, 7 weeks, ~20 g) were purchased from the Changzhou Cavens Biological Technology Co, Ltd., and allowed to acclimatize for 1 week in the laboratory. All animal procedures were performed in accordance with the Guidelines for Care and Use of Laboratory Animals of Shandong University and approved by the Animal Ethics Committee of Shandong University. After the mice were anesthetized by intraperitoneal injection of chloral hydrate, a 1.2 \times 1.2 cm² round full-thickness wound was made on the back of the mice, and the wound was fixed with splint to prevent the wound from acute contraction. Finally, the biofilm was formed by *in situ* inoculation of *S. aureus* 10⁷ CFU/mL on the wound surface for 2 days.

Treatment of *S. aureus*-infected wounds. Mice were divided into 5 groups with 5 mice in each group: PBS, Collagen, GR, GR + CuS + IR, GR+ CuS + IR + Col. Recombinant human collagen type III (gel) was mixed with antimicrobial peptide hydrogel to form a “double network” hybrid hydrogel dressing for wound treatment. The concentration of CuS NDs is 1 mg/mL, and the 6 min was irradiated by NIR laser (808 nm, 1.8W / cm²). Each group was given new corresponding samples (100 μL) every day without removing the remaining samples from the previous day and stopped on the 5th day, and the wound healing of mice was recorded every day. Ten days later, the mice were killed to take the skin tissue from the wound for bacterial culture. Then hematoxylin-eosin (H&E) staining, Masson’s trichrome staining, Gram staining, immunofluorescence technique and immunohistochemical CD31 staining were used to evaluate the effect of bacterial clearance and healing of wounds in each group. In addition, the skin wound, blood, liver, spleen and kidney were digested with aqua regia. The digestive juice was diluted with DI water and filtered with 0.22 μm filter membrane. Copper content was measured by inductively coupled plasma mass spectrometer (ICP-MS, NexION 350X, PerkinElmer, USA).

Results and Discussion

Synthesis and Characterization of Antimicrobial Peptide Hydrogel. To obtain peptide hydrogel with inherent antibacterial activity, we designed AMP-RADA₁₆ fusion peptide (IKKIIKKIKKIIGGRADARADARADARADA-NH₂), denoted as GR peptide, in which antimicrobial peptide was connected to RADA₁₆ through a glycine (G) linker.^{27,28} The GR peptide was synthesized by Fmoc solid-phase peptide synthesis, and confirmed by mass spectrometry after purification by HPLC (Figure S1 and Figure S2). The GR peptide gels at a concentration of 2% (w/v) in the presence of 0.9% NaCl (w/v), and the intertwined nanofiber structure of hydrogel can be observed by TEM and AFM), which provides an ideal network to encapsulate drugs (Figure 1A and Figure S3). In addition, this conclusion was also proved by the effective loading of hydrophobic Cypate, hydrophilic Cy5 or CuS nanodots in GR hydrogels (Figure 1B).

The viscoelasticity of the formed GR hydrogel was evaluated based on oscillatory rheology. At the frequency of 0.1-100 Hz, the storage modulus (G') is always higher than the loss modulus (G'') at a constant strain of 0.1%, indicating the solid-like gel materials have good

mechanical properties (Figure 1C). To confirm the injectability of gelatinous materials, a time-dependent step-strain rheological experiment was performed. When amplitude oscillation strain was increased by 40%, the G' value decreases sharply and is lower than G'' instantly, and the GR gel remains quasi-liquid under continuous deformation. In this continuous testing process, when the applied strain is restored to 0.1%, both G' and G'' fully return to their original values immediately, and the process is repeatable (Figure 1D). These results show that both injection and smear of GR hydrogel can fill the wound completely, which can support different clinical applications.

The secondary structure of GR was probed by FT-IR spectroscopy. The FT-IR spectrum of the GR gel in physiological saline showed two intense peaks at 1630 and 1649 cm^{-1} in the amide-I region, suggesting intermolecular antiparallel β -sheet arrangement among the gelating molecules (Figure 1E).²⁹ Meanwhile, compared to the FT-IR spectrum of GR in solution phase, the redshifted peak of carboxyl was observed in the corresponding gel phase, demonstrating the presence of intermolecular hydrogen bonding in the formed hydrogel (Figure S4).³⁰ Moreover, the fluorescence spectrum of GR hydrogel showed an emission peak at 311 nm, which indicated that there was π - π accumulation between amino acid residues, enhancing the gelation of the hydrogel (Figure 1F).²⁹

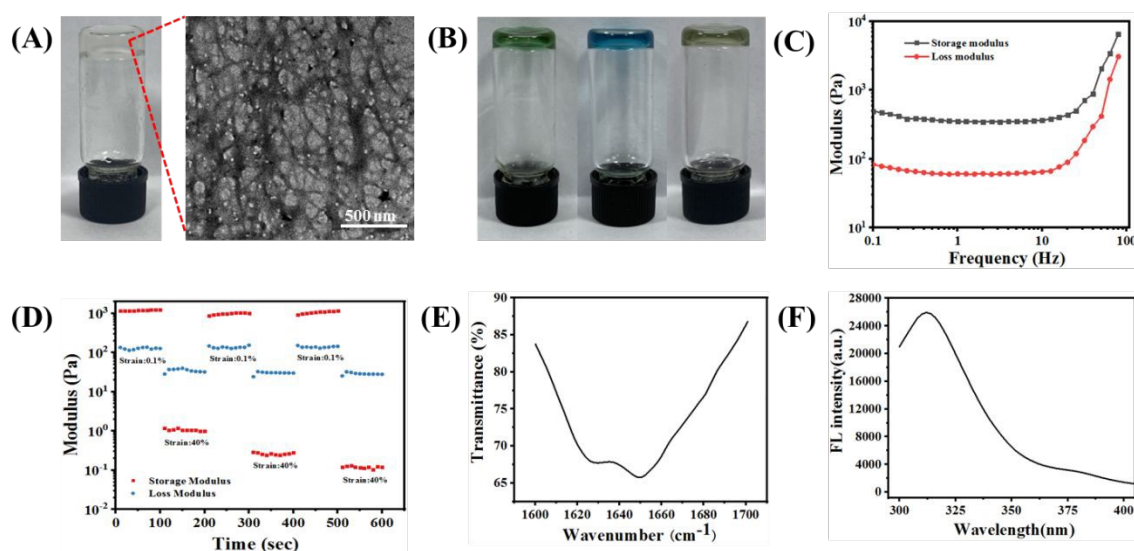


Figure 1. Preparation and characterization of GR hydrogel. (A) TEM images of GR hydrogel. (B) Photos of GR hydrogel loaded with various reagents (Cypate, Cy5 and CuS NDs). (C) Storage modulus (G') and loss modulus (G'') of GR hydrogel with frequency

change. (D) Storage modulus (G') and loss modulus (G'') change with cyclic strain. (E) FT-IR spectra of GR hydrogel. (F) Fluorescence spectra of GR hydrogel.

Synthesis and Related Photothermal Properties of CuS Nanodots. CuS NDs were prepared by a simple one-pot synthesis according to the existing method.³¹ The reaction conditions are relatively mild, and the final product is a dark green solution. Using transmission electron microscopy (TEM), we found the obtained CuS NDs have a relatively uniform size distribution with a diameter of about 9 nm, which is similar as the hydrated particle size (10 ± 1.2 nm) measured by DLS (Figure 2A). This means that the particles can fit in the cavity of the hydrogel. Meanwhile, the hydrated particle size of CuS NDs remained unchanged for at least 7 days, showing its stability under physiological conditions (Figure 2B). The CuS NDs showed absorption in near infrared range of 600 - 1000 nm (Figure 2C), which means it is likely a photothermal agent (PTA) that may have photothermal effect with NIR irradiation. No significant change of the absorption spectra was observed after NIR irradiation, suggesting that CuS NDs are photostable.

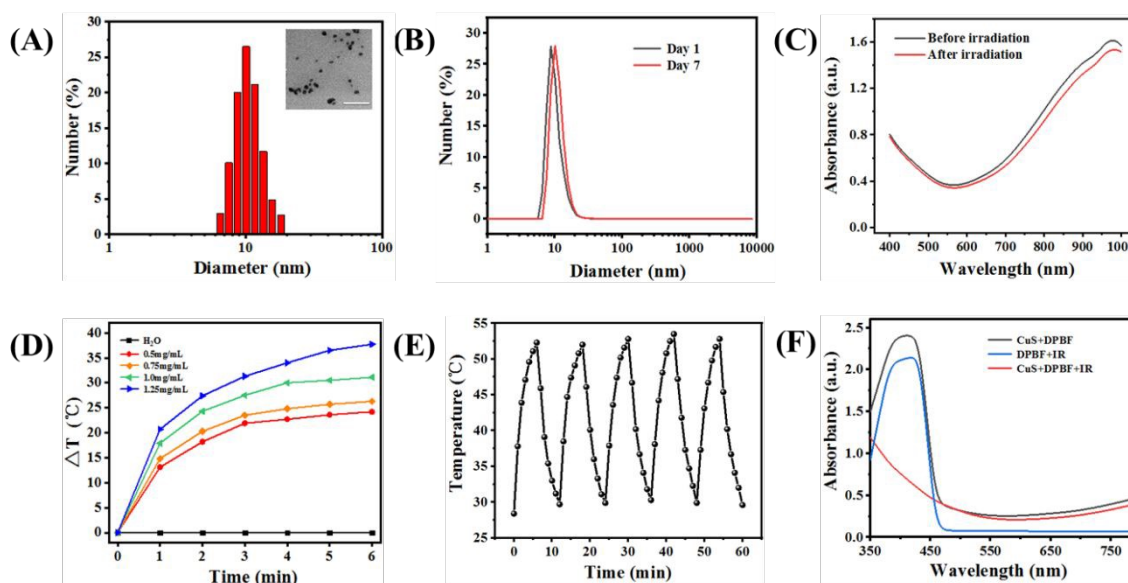


Figure 2. (A) Particle size and TEM image of CuS NDs. The scale bar represents 50 nm. (B) 7-day particle size change of CuS NDs. (C) Visible light absorption curve of CuS NDs before and after NIR irradiation (808 nm, 1.8 W/cm²). (D) Concentration-dependent temperature changes of CuS NDs under 808 nm laser irradiation (1.8 W/cm²). (E) Temperature changes of CuS NDs (1 mg/mL) during five on/off cycles of laser irradiation (1.8 W/cm²). (F) Absorption spectra of DPBF before and after adding CuS NDs (1 mg/mL) and NIR irradiation (808 nm, 1.8 W/cm²).

We next measured the photothermal behavior of CuS NDs with irradiation by NIR laser (808 nm, 1.8 W/cm²). Under NIR irradiation, a rapid temperature rise was observed at lower concentration of the particle (0.5 mg/mL) and became more pronounced with increasing particle concentration. At 1.25 mg/mL, we observed a remarkable temperature increase of more than 35 °C in 5 min. The photothermal effect also increases with the power of NIR laser (Figure 2D and Figure S5). The photothermal effect was also reversible: stable temperature rise over five heating-cooling cycles was observed without compromise of the photothermal effect (Figure 2E). Using DPBF as an indicator, we also measured the generation of ROS. As shown in Figure 2F, after co-incubation with CuS NDs, the absorption of DPBF decreased significantly following NIR irradiation.^{32,33}

Antibacterial activity *in vitro*. We next measured the bacterial killing activity of the GR hydrogel against a Gram-positive (G+ve) bacterium *Staphylococcus aureus* (*S. aureus*) and Gram-negative (G-ve) bacterium *Escherichia coli* (*E. coli*). Briefly, bacterial cultures (10⁸ CFU/mL) were incubated with different concentration of GR hydrogels, and the cell viability was quantified after 1 h treatment. As shown in Figure 3, GR hydrogel effectively kills both bacteria in a concentration-dependent manner. Interestingly, the antibacterial peptide hydrogel is significantly more effective towards the G-ve *E. coli* than G+ve *S. aureus*. At GR hydrogel concentration of 10 μM, more than 99.9% of the *E. coli* culture was killed, whereas the MIC₅₀ of GR hydrogel towards *S. aureus* was around 20 μM. The reason of this selectivity remains unknown. We then measured the cytotoxicity of the GR hydrogel using *L929s* and MTT assay. After 24 hours of culture, the survival rate of cells at a concentration of 48 μM (higher than the bacterial MIC₉₀) was still greater than 80% (Figure 3C). With TritonX-100 as a positive control, the hemolysis rate was calculated quantitatively. At 40 μM, the hydrogel exhibited a hemolysis rate less than 1% (Figure 3F). This result indicates that the antibacterial peptide sequence maintained the bactericidal activity despite covalent conjugation with a gel formation peptide or physical crosslinking to a gel form. The peptide hydrogel is also non-harmful to mammalian cells and red blood cells.

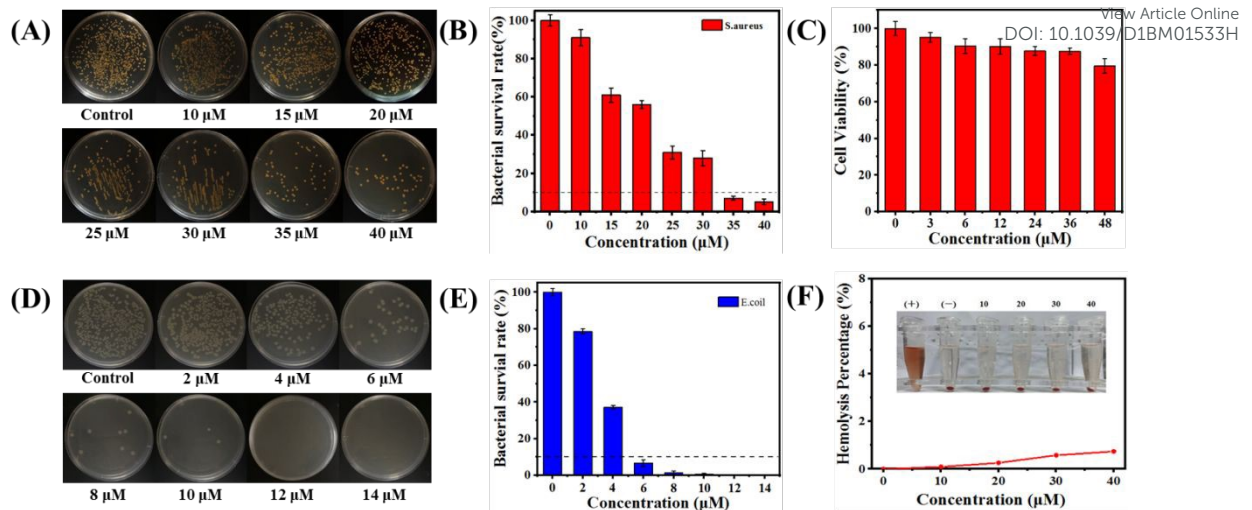


Figure 3. Colony images (A) and statistical chart (B) of *S. aureus* incubated with different concentrations of GR hydrogel. (C) Cytotoxicity of different concentrations of GR hydrogel incubated with *L929s* cells. Colony images (D) and statistical chart (E) of *E. coli* incubated with different concentrations of GR hydrogel. (F) Hemolysis rate and image of red blood cells incubated with different concentrations of GR hydrogel.

Next, we focused on the inhibitory effect of GR hydrogel on the G+ve *S. aureus*. When we co-cultured *S. aureus* with GR hydrogel, the proliferation of *S. aureus* was significantly inhibited within 12 h (Figure 4A). Therefore, although the hydrogel did not eradicate the bacterial cells, it can suppress the growth of the cells. Then we used crystal violet staining to explore whether GR hydrogel could inhibit biofilm formation. GR hydrogel and *S. aureus* were incubated together for 2 days and then treated with crystal violet. Encouragingly, we can hardly see purple staining in the bacterial culture incubated with hydrogel and 90% of biofilm formation was inhibited (Figure 4B). In live/dead staining experiments, we used the red fluorescence dye PI to stain dead bacterial cells and the green fluorescence dye SYTO 9 to stain red bacterial cells. It was observed all the bacterial cells incubated with GR hydrogel showed red fluorescence, which indicated that GR exhibited excellent bactericidal activity (Figure 4C).³⁴ Therefore, although GR hydrogel is more effective in killing *E. coli*, it can also effectively suppress the growth of *S. aureus* and cause cell lysis.

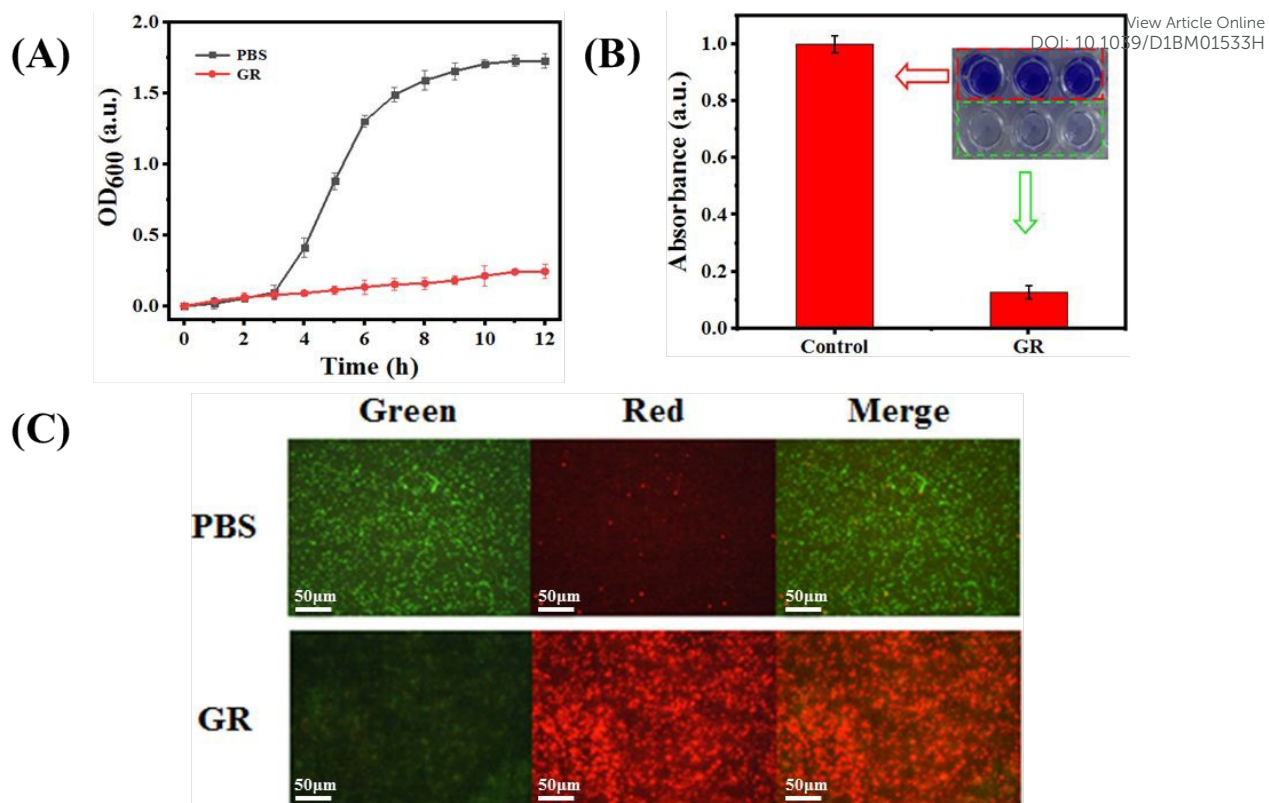


Figure 4. (A) Effect of GR hydrogel on the growth curve of *S. aureus*. (B) GR hydrogel inhibits the formation of crystal violet staining image and absorbance of *S. aureus* biofilm. (C) Fluorescent images of live/dead staining of *S. aureus* co-incubated with GR hydrogel.

Antibacterial Activity of CuS NDs-loaded Hydrogel. Next we loaded CuS NDs into GR hydrogel and measured the antibacterial activity under NIR irradiation. When we irradiate the composite hydrogel with near-infrared light (808 nm, 1.8 W/cm²), the photothermal effect was unchanged as compared with CuS NDs alone (Figures 5A and Figure 5B). At the concentration of 20 μM (MIC₅₀ of the GR hydrogel for *S. aureus*), we observed that the ND-doped hydrogel could completely eradicate the bacterial cells (Figure 5C and Figure 5D). Therefore, although CuS NDs showed comparable antibacterial activity to GR hydrogel due to the release of Cu²⁺,^{22,35} their combination showed significantly added effect towards *S. aureus*. It may be due to the overlap between the thermal radiation range and the diffusion region of the two components, irradiation did not significantly change the diameter of the bacteriostatic zone in the agar disk diffusion experiment (Figure S6). Because the components of the biofilm including lipopolysaccharide, protein, and DNA are sensitive to heat, CuS NDs-based photothermal therapy further improves the breakage effect of the intact biofilm (Figure S7).

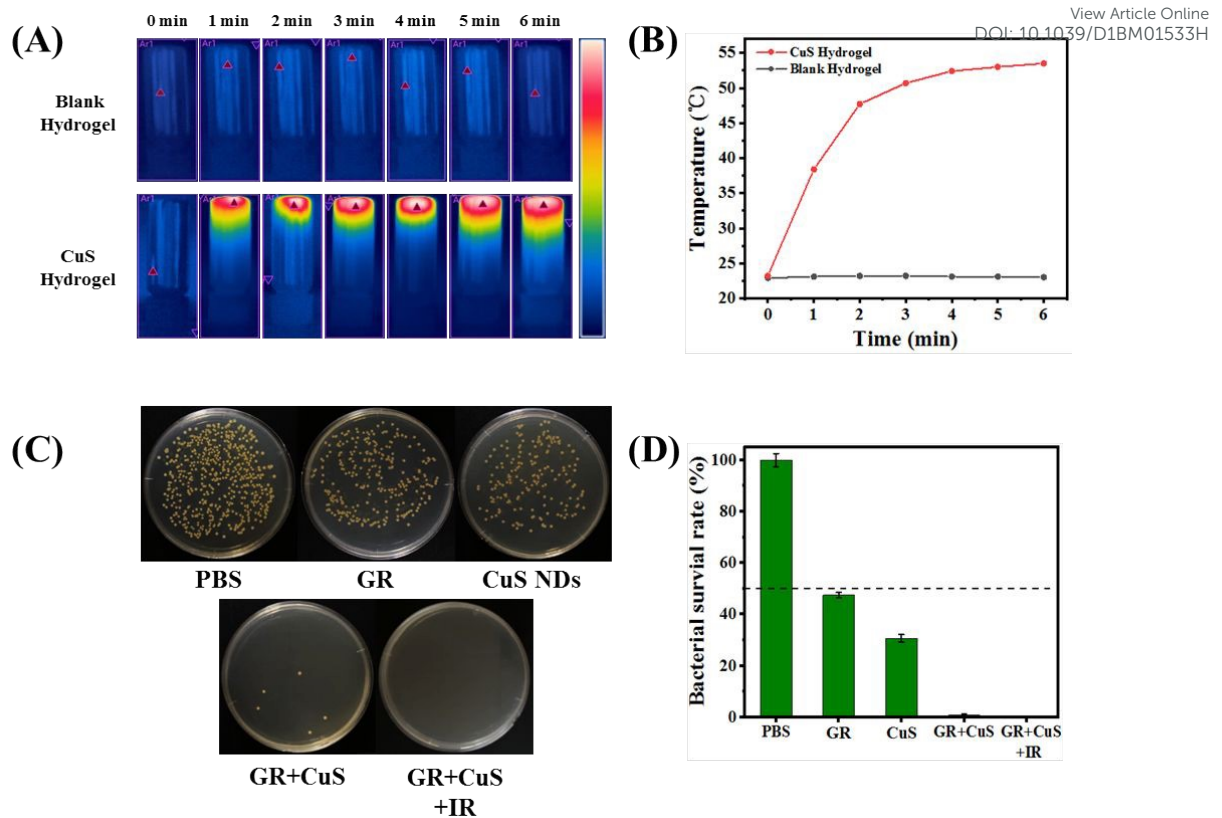


Figure 5. The heating images (A) and temperature curves (B) of CuS NDs-loaded (1 mg/mL) hydrogels and blank hydrogels in 6 min irradiated by NIR (808 nm, 1.8 W/cm²). Colony images (C) and statistical chart (D) of killing *S. aureus* under different components and NIR irradiation.

Antibacterial activity *in vivo* and wound healing. Lastly, we measure the antibacterial effect against *S. aureus* and the promotion of the healing of infected wounds in BALB/c mice. As shown in Figure 6A, a 1.2 × 1.2 cm² full-thickness wound was made on the back of mice, and a circular splint was sutured on the wound to prevent the rapid closure of the aponeurosis to the wound. *S. aureus* infection was used to simulate severe injury and infection of the wound. To further accelerate the wound healing, we also added collagen with GR hydrogel. All the animals were randomly divided into 5 groups: PBS, collagen, GR, GR + CuS + IR, GR + CuS + IR + Col. In the irradiation group, 6 min irradiation with NIR (808 nm, 1.8 W/cm²) each day was implemented, and the wound temperature was maintained at 45-50 °C, which does not cause damage to healthy tissues (Figure S8). Figure 6B shows a representative image of the wound treated from 0 to 10 days. In the previous week, the wound of each group was covered with scar tissue, and the scar treated with collagen was thinner. On the 8th day, the scar and splint in the irradiation group fell off from the wound, showing a faster healing rate. At day 10, the wound in GR + CuS + IR + Col group has

almost completely healed, leaving only a scar on the surface of the skin. The combination therapy therefore accelerates wound healing and closure.

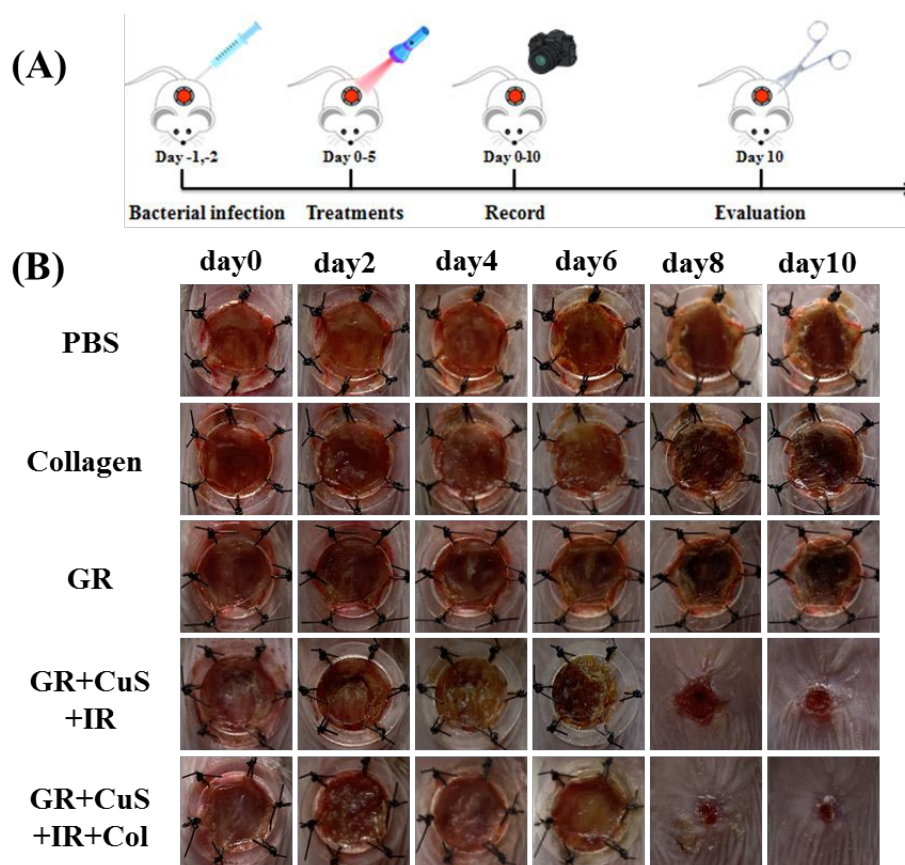


Figure 6. (A) Schematic illustration of the operation of wound establishment, treatment and examination. (B) The images of infected mice treated with 5 different treatment groups (PBS, Collagen, GR, GR + CuS + IR, GR + CuS + IR + Col) for 10 days.

Subsequently, we analyzed the infection states of the wounds at day 10. Mice were sacrificed and dissected, and the skin wound tissue was homogenized and inoculated on the agar plate. Consistent with the results of wound healing, the hydrogel group showed a limited germicidal effect, possibly due to the protective effect of biofilm on the wound surface. The irradiation group showed complete bacterial clearance. Gram staining of skin tissue sections supported this conclusion, as no signs of gram-positive bacterial cells were observed in the irradiation group (Figure 7). This result shows that the antibacterial activity correlates with the wound healing process.

Lastly, the quality of wound healing was evaluated by hematoxylin-eosin staining (H&E), Masson's trichrome staining and tissue immunofluorescence assays. According to the results of H&E staining, only GR + CuS + IR + Col showed complete re-epithelialization. Although

the skin tissues from other irradiation groups were deprived of severe ulceration, they were also accompanied with adverse conditions such as blisters (Figure 8A). According to Masson staining, samples from the three groups without irradiation showed loose tissue structures with relatively low collagen formation. Dense collagen fibers were found to be deposited in the samples from the irradiation group, but the collagen fibers in the GR + CuS + IR + Col group were thicker and more regularly arranged (Figure 8B). Similarly, samples from the GR + CuS + IR + Col group showed more angiogenesis (red) in CD31 immunofluorescence, which also meant that more nutrients and oxygen were delivered to the wound bed to benefit the wound healing (Figure 8C). The results of CD31 immunohistochemical staining (red arrows) also reached a similar conclusion (Figure 8D). Moreover, no structural changes were found in the main organs of each treatment group, and copper was mainly concentrated in the wound tissue. All these results suggest that our materials are safe (Figure S9 and Figure S10). Altogether, bacterial clearance promotes neovascularization and accelerates the rapid, complete healing of the wound.

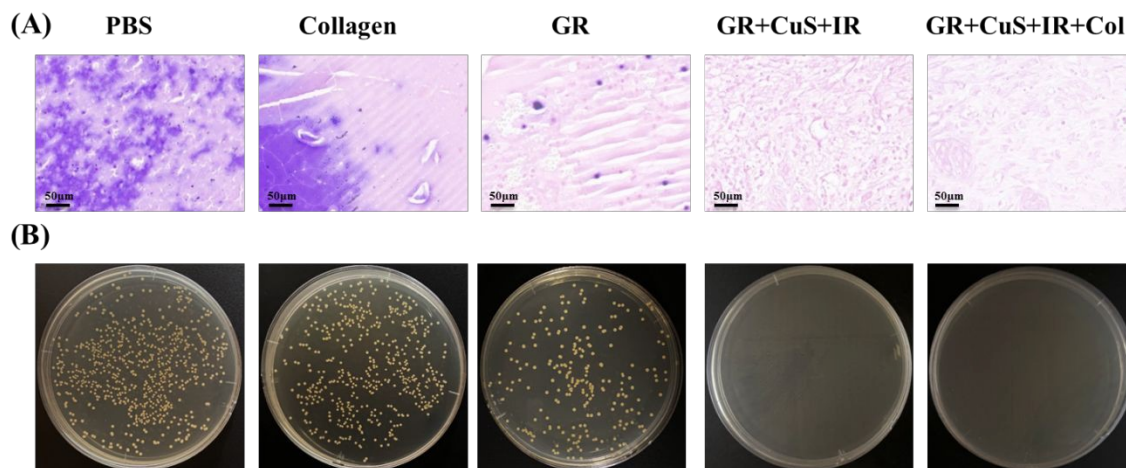


Figure 7. (A) Gram staining images of skin tissue of mice infected with *S. aureus* in each treatment group were treated for 10 days. (B) The image of plate colony in the skin of mice infected with *S. aureus* in each treatment group.

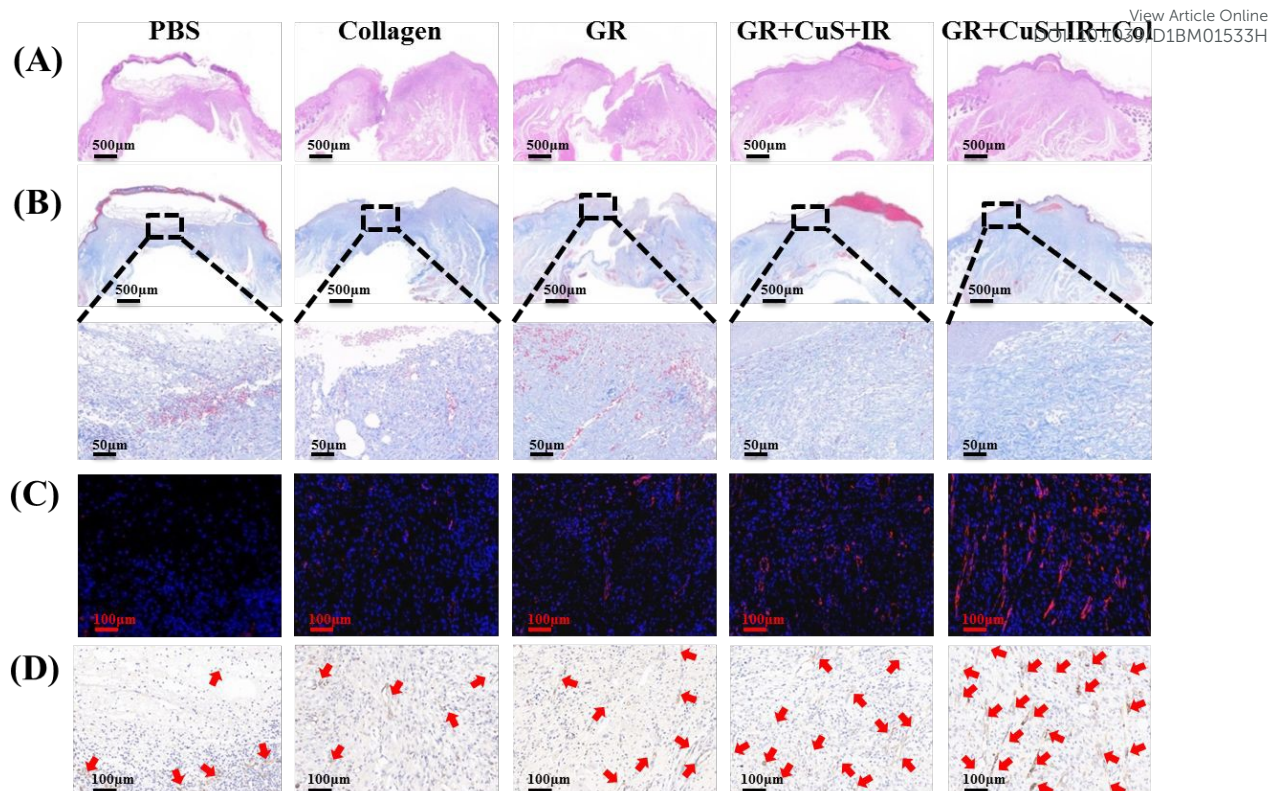


Figure 8. H&E staining (A), Masson staining (B), CD31 immunofluorescence (C) and CD31 immunohistochemical (D) image of skin tissue of mice infected with *S. aureus* in each treatment group were treated for 10 days.

Conclusion

In this work, we developed a GR peptide hydrogel with broad-spectrum antibacterial activity and good biocompatibility, which harnesses both the antibacterial activity of CuS NDs and antimicrobial peptide hydrogel to treat severe wound infection and promote wound healing. The GR peptide hydrogel eradicates bacterial colonies or suppresses bacterial growth. CuS NDs exert outstanding antibacterial activity by emitting ROS and photothermal effect under NIR irradiation. Doping CuS NDs in GR hydrogel produces a hybrid material with outstanding bacterial killing activity both *in vitro* and in a wound infection model of mice. Together with a layer of collagen, the ND-doped hydrogel effectively eradicated *S. aureus* in the infected wounds and promoted a rapid wound closure under NIR irradiation. This work thereby showcases a combination of contact-based antimicrobial peptide hydrogel and non-contact based photodynamic and photothermal effects to exert antibacterial activity. The protocol may prove to be an effective infection control strategy in vulnerable patients.

Data Availability Statement

All data are exhibited in the main text or the SI Appendix.

View Article Online
DOI: 10.1039/D1BM01533H

ACKNOWLEDGEMENT

We acknowledge funding support by Jiangsu Key Research and Development Plan (Society Development, No. BE2018639), the QingLan Project of Jiangsu Province, the Science & Technology Support Program of Changzhou (Application Basic Research, No. CJ20210142), the Research Grants Council of Hong Kong (N_CUHK422/18) and a CUHK-University of Manchester Joint Grant (Seed-corn Fund RAC-2019/20). We also acknowledge the help of Hong Chai from Analysis and Testing Center, NERC Biomass of Changzhou University in FT-IR experiment.

Competing interest statement: The authors declare no competing interests.

Author contributions: J. Wang, X. Ni and J. Xia designed research and provided the funding; X. Wang and L. Qiu performed research; X. Wang and C. Wang wrote the paper and C. Wang provided the funding, Z. Gao, S. Zhou, P. Cui, H. Hu, P. Jiang, X. Du analyzed data.

References

- 1 E. Levesque, Y. Feng, R. A. Jones and P. Martin, Inflammation Drives Wound Hyperpigmentation in Zebrafish by Recruiting Pigment Cells to Sites of Tissue Damage, *Dis. Models Mech.*, 2013, **6**, 508-515.
- 2 A. K. Dąbrowska, F. Spano, S. Derler, C. Adlhart, N. D. Spencer and R. M. Rossi, The Relationship between Skin Function, Barrier Properties, and Body-Dependent Factors, *Skin Res. Technol.*, 2018, **24**, 165-174.
- 3 X. Lei, L. Qiu, M. Lan, X. Du, S. Zhou, P. Cui, R. Zheng, P. Jiang, J. Wang and J. Xia, Antibacterial Photodynamic Peptides for Staphylococcal Skin Infection, *Biomater. Sci.*, 2020, **8**, 6695-6702.
- 4 G. C. Gurtner, S. Werner, Y. Barrandon and M. T. Longaker, Wound Repair and Regeneration, *Nature*, 2008, **453**, 314-321.

- 5 B. K. Sun, Z. Siprashvili and P. A. Khavari, Advances in Skin Grafting and Treatment of Cutaneous Wounds, *Science*, 2014, **346**, 941-945.
- 6 J. Wang, X. Chen, Y. Zhao, Y. Yang, W. Wang, C. Wu, B. Yang, Z. Zhang, L. Zhang, Y. Liu, X. Du, W. Li, L. Qiu, P. Jiang, X. Mou and Y. Li, pH-Switchable Antimicrobial Nanofiber Networks of Hydrogel Eradicate Biofilm and Rescue Stalled Healing in Chronic Wounds, *ACS Nano*, 2019, **13**, 11686–11697.
- 7 A. Bhatia, K. O'Brien, M. Chen, A. Wong, W. Garner, D. T. Woodley and W. Li, Dual Therapeutic Functions of F-5 Fragment in Burn Wounds: Preventing Wound Progression and Promoting Wound Healing in Pigs, *Mol. Ther.-Methods Clin. Dev.*, 2016, **3**, 16041.
- 8 K. Chae, W. Y. Jang, K. Park, J. Lee, H. Kim, K. Lee, C. K. Lee, Y. Lee, S. H. Lee and J. Seo, Antibacterial Infection and Immune-Evasive Coating for Orthopedic Implants, *Sci. Adv.*, 2020, **6**, eabb0025.
- 9 L. Zhou, H. Zheng, Z. Liu, S. Wang, Z. Liu, F. Chen, H. Zhang, J. Kong, F. Zhou and Q. Zhang, Conductive Antibacterial Hemostatic Multifunctional Scaffolds Based on $Ti_3C_2T_x$ MXene Nanosheets for Promoting Multidrug-Resistant Bacteria-Infected Wound Healing, *ACS Nano*, 2021, **15**, 2468-2480.
- 10 J. Wang, H. Wu, Y. Yang, R. Yan, Y. Zhao, Y. Wang, A. Chen, S. Shao, P. Jiang and Y. Li, Bacterial Species-Identifiable Magnetic Nanosystems for Early Sepsis Diagnosis and Extracorporeal Photodynamic Blood Disinfection, *Nanoscale*, 2018, **10**, 132-141.
- 11 C. Thompson, R. Verani, G. Evanoff and E. Weinman, Suppurative Bacterial Pyelonephritis as a Cause of Acute Renal Failure, *Am. J. Kidney Dis.*, 1986, **8**, 271-273.
- 12 M. E. Falagas, G. S. Tensarli, D. E. Karageorgopoulos and K. Z. Vardakas, Deaths Attributable to Carbapenem-Resistant Enterobacteriaceae Infections, *Emerg. Infect. Dis.*, 2014, **20**, 1170-1175.
- 13 S. B. Levy and B. Marshall, Antibacterial Resistance Worldwide: Causes, Challenges and Responses, *Nat. Med.*, 2004, **10**, S122-S129.
- 14 J. Davies and D. Davies, Origins and Evolution of Antibiotic Resistance, *Microbiol. Mol. Biol. Rev.*, 2010, **74**, 417-433.
- 15 M. E. A. de Kraker, A. J. Stewardson and S. Harbarth, Will 10 Million People Die a Year Due to Antimicrobial Resistance by 2050? *PLoS Med.*, 2016, **13**, e1002184.
- 16 J. Vila, J. Moreno-Morales and C. Balleste-Delpierre, Current Landscape in The Discovery of Novel Antibacterial Agents, *Clin. Microbiol. Infect.*, 2020, **26**, 596-603.

- 17 Q. Zheng, X. Liu, Y. Zheng, K. W. K. Yeung, Z. Cui, Y. Liang, Z. Li, S. Zhu, X. Wang and S. Wu, The Recent Progress on Metal–Organic Frameworks for Phototherapy, *Chem. Soc. Rev.*, 2021, **50**, 5086-5125.
- 18 Y. Ren, H. Liu, X. Liu, Y. Zheng, Z. Li, C. Li, K. W. K. Yeung, S. Zhu, Y. Liang, Z. Cui and S. Wu, Photoresponsive Materials for Antibacterial Applications, *Cell Rep. Phys. Sci.*, 2020, **1**, 100245.
- 19 X. Kong, X. Liu, Y. Zheng, P. K. Chu, Y. Zhang and S. Wu, Graphitic Carbon Nitride-Based Materials for Photocatalytic Antibacterial Application, *Mater. Sci. Eng. R*, 2021, **145**, 100610.
- 20 Y. X, X. Liu, Y. Zheng, C. Li, K. W. K. Yeung, Z. Cui, Y. Liang, Z. Li, S. Zhu and S. Wu, Ag₃PO₄ Decorated Black Urchin-Like Defective TiO₂ for Rapid and Long-term Bacteria-Killing under Visible Light, *Bioact. Mater.*, 2021, **6**, 1575-1587.
- 21 J. Huang, J. Zhou, J. Zhuang, H. Gao, D. Huang, L. Wang, W. Wu, Q. Li, D. Yang and M. Han, Strong Near-Infrared Absorbing and Biocompatible CuS Nanoparticles for Rapid and Efficient Photothermal Ablation of Gram-Positive and -Negative Bacteria, *ACS Appl. Mater. Interfaces*, 2017, **9**, 36606-36614.
- 22 D. Han, P. Yu, X. Liu, Y. Xu and S. Wu, Polydopamine Modified CuS@HKUST for Rapid Sterilization through Enhanced Photothermal Property and Photocatalytic ability, *Rare Met.*, 2021, DOI: 10.1007/s12598-021-01786-1.
- 23 C. Wang, T. Hong, P. Cui, J. Wang and J. Xia, Antimicrobial Peptides towards Clinical Application: Delivery and Formulation, *Adv. Drug Deliv. Rev.*, 2021, **175**, 113818.
- 24 R. E. W. Hancock and H. G. Sahl, Antimicrobial and Host-Defense Peptides as New Anti-Infective Therapeutic Strategies, *Nat. Biotechnol.*, 2006, **24**, 1551-1557.
- 25 L. Qiu, C. Wang, X. Lei, X. Du, Q. Guo, S. Zhou, P. Cui, T. Hong, P. Jiang, J. Wang, Y. Li and J. Xia, Gelatinase-Responsive Release of an Antibacterial Photodynamic Peptide against *Staphylococcus aureus*, *Biomater. Sci.*, 2021, **9**, 3433.
- 26 L. Qiu, C. Wang, M. Lan, Q. Guo, X. Du, S. Zhou, P. Cui, T. Hong, P. Jiang, J. Wang and J. Xia, Antibacterial Photodynamic Gold Nanoparticles for Skin Infection, *ACS Appl. Bio Mater.*, 2021, **4**, 3124-3132.
- 27 C. Chen, J. Hu, P. Zeng, Y. Chen, H. Xu and J. Lu, High Cell Selectivity and Low-Level Antibacterial Resistance of Designed Amphiphilic Peptide G(IKK)₃I-NH₂, *ACS Appl. Mater. Interfaces*, 2014, **6**, 16529-16536.

- 28 H. Yokoi, T. Kinoshita and S. Zhang, Dynamic Reassembly of Peptide RADA₁₆ Nanofiber Scaffold, *Proc. Natl. Acad. Sci. U. S. A.*, 2005, **102**, 8414-8419.
- 29 G. Ghosh, R. Barman, J. Sarkar and S. Ghosh, pH-Responsive Biocompatible Supramolecular Peptide Hydrogel, *J. Phys. Chem. B*, 2019, **123**, 5909-5915.
- 30 I. Irwansyah, Y. Li, W. Shi, D. Qi, W. R. Leow, M. B. Y. Tang, S. Li and X. Chen, Gram-Positive Antimicrobial Activity of Amino Acid-Based Hydrogels, *Adv. Mater.*, 2015, **27**, 648-654.
- 31 J. Fu, J. Zhang, S. Li, L. Zhang, Z. Lin, L. Liang, A. Qin and X. Yu, CuS Nanodot-Loaded Thermosensitive Hydrogel for Anticancer Photothermal Therapy, *Mol. Pharm.*, 2018, **15**, 4621-4631.
- 32 Y. Qiao, Y. Ping, H. Zhang, B. Zhou, F. Liu, Y. Yu, T. Xie, W. Li, D. Zhong, Y. Zhang, K. Yao, H. A. Santos and M. Zhou, Laser-Activatable CuS Nanodots to Treat Multidrug-Resistant Bacteria and Release Copper Ion to Accelerate Healing of Infected Chronic Nonhealing Wounds, *ACS Appl. Mater. Interfaces*, 2019, **11**, 3809-3822.
- 33 W. Zhang, B. Li, H. Ma, L. Zhang, Y. Guan, Y. Zhang, X. Zhang, P. Jing and S. Yue, Combining Ruthenium(II) Complexes with Metal-Organic Frameworks to Realize Effective Two-Photon Absorption for Singlet Oxygen Generation, *ACS Appl. Mater. Interfaces*, 2016, **8**, 21465-21471.
- 34 Y. Yu, L. Tan, Z. Li, X. Liu, Y. Zheng, X. Feng, Y. Liang, Z. Cui, S. Zhu and S. Wu, Single-Atom Catalysis for Efficient Sonodynamic Therapy of Methicillin-Resistant Staphylococcus aureus-Infected Osteomyelitis, *ACS Nano*, 2021, **15**, 10628-10639.
- 35 R. Lv, Y. Liang, Z. Li, S. Zhu, Z. Cui and S. Wu, Flower-Like CuS/Graphene Oxide with Photothermal and Enhanced Photocatalytic Effect for Rapid Bacteria-Killing Using Visible Light, *Rare Met.*, 2021, DOI: 10.1007/s12598-021-01759-4.